Title
VSP Site Characterization at NTS - Summary Report

Authors
Daley, T.M.
McEvilly, T.V.
Michelini, A.

Publication Date
1990-10-01

LBL-29778
UC-403

Lawrence Berkeley Laboratory
UNIVERSITY OF CALIFORNIA

EARTH SCIENCES DIVISION

VSP Site Characterization at NTS—Summary Report

T.M. Daley, T.V. McEvilly, and A. Michelini

October 1990

Prepared for the U.S. Department of Energy under Contract Number DE-AC03-76SF00098.

DISCLAIMER

LBL-29778

VSP Site Characterization at NTS—Summary Report

T. M. Daley, T. V. McEvilly, and A. Michelini

Earth Sciences Division
Lawrence Berkeley Laboratory
University of California
Berkeley, California 94720

October 1990

This work was done at the Lawrence Berkeley Laboratory under the auspices of the U.S. Department of Energy Lawrence Livermore Laboratory under Contract No. W-7405-ENG-48. Data processing was done at the Lawrence Berkeley Laboratory Center for Computational Seismology under U.S. Department of Energy Contract No. DE-AC03-76SF00098.

Introduction

In late 1989 a site characterization study using the Vertical Seismic Profile (VSP) method was conducted as part of the On Site Seismic Yield (OSSY) experiment organized by Lawrence Livermore Laboratory at well UE-10 ITS #3 located in Yucca valley inside the Nevada Test Site (NTS). The OSSY experiment fired 10 and 100 lb explosive sources at several depths in the hole, with multiple 3-component receivers on the surface, to test the nature of seismic signal scaling with source size and the accuracy in the near field of source modeling algorithms. Shear-waves in particular are influenced strongly by both the source mechanism and the properties of the propagation path. The multi-component OSSY VSP (3-component receivers at several depths, with P, SV and SH surface sources) measured the seismic wave transmission separately for three source types. The VSP surface-source to borehole-receiver acquisition geometry was reversed in the subsequent explosion phase of the experiment in which the explosion-generated waves presumably experienced the same propagation effects as did the waves generated by the VSP sources.

The OSSY VSP has progressed through data acquisition and processing to an initial interpretation in terms of P- and S-velocity structures. Preliminary results were presented at the 1990 meeting of the Seismological Society of America (Daley and McEvilly, 1990). This report is an overview of the data acquisition, processing and analysis to date, and on plans for the next phase of interpretation.

Survey Design

The OSSY VSP experiment has the following goals:

1) Record waveforms along reciprocal raypaths of the OSSY explosions, with 3-component sensors and for three source force orientations.
2) Develop a 3-D P- and S-velocity model for source modeling of subsequent explosions in the borehole.
3) Investigate possible seismic anisotropy in the explosive source region and near the well.
4) Detect and map in 3-D any strong structural heterogeneity near the well.
5) Measure the attenuation (Q) near the well and its frequency dependence if evident.

The multi-offset VSP survey was designed to address these goals. The VSP sources, located at the same surface sites as receivers for the subsequent OSSY explosions, were offset 0 to 1200 m on four azimuths, with at least two source points on each azimuth (Figure 1a.). At each source point we acquired three vibrator data sets, P-source, SV- and SH-source, using an 8-80 Hz sweep with four seconds of correlated data at 2 millisecond sampling. The 3-component VSP receiver was positioned at recording depths clustered around the planned explosion depths to a maximum depth of 600 m (Figure 1b).

Data Acquisition

The data acquisition was performed in a novel circular 'racetrack' method which allowed the receiver to remain locked at one depth while all the source points were vibrated. This was accomplished by having 2 pairs (one P, one S) of vibrators in separate 'tracks' through the pattern of offsets, alternating operation until the 3 sources for each receiver depth were obtained at all the source points. This method insured consistent receiver response since the borehole geophone was not reclamped for each source point (the usual VSP procedure is to record all depths for one source location and then move the source). At least 4 sweeps were recorded for each source (usually 6). Initial processing, including correlation and sorting into depth-ordered common source point data sets, was performed by the contractor, Seismograph Service Corporation. Further processing at the Center for Computational Seismology (CCS) at Lawrence Berkeley Laboratory (LBL) included editing of bad traces, sorting by source type at each source location, stacking of individual sweeps, and converting horizontal components to a consistent coordinate system.

Data Analysis

The initial step of data analysis was a single joint estimation of horizontal receiver component orientation for each receiver level. Because the borehole geophone rotates around the vertical axis as it moves from level to level, there is no control of the orientation of the horizontal components. An eigenvector analysis of the cross-covariance matrix for the 3-component recording of the initial P-wave arrival gives the orientation of the 3-component receiver with respect to the P-wave raypath. The receiver orientation with respect to north is thus determined if the P-wave raypath stays in the vertical plane of incidence. For the OSSY experiment's multiple source-receiver paths we computed an average orientation at each receiver depth using P-waves from all the source points, since the receiver remained clamped while all the sources were vibrated. This joint solution yielded a horizontal orientation at all 35 receiver depths with an average standard deviation of 9.5 degrees. An interesting result of this orientation exercise was the apparent bending of raypaths out of the azimuthal plane (as defined by the other eight sites) for arrivals from the northwest sites (9 and 13, Figure 1a). This finding indicates subsurface lateral heterogeneity to the northwest.

Given the horizontal component orientations, the raw waveform data are 'rotated' into a consistent coordinate system. This 'borehole' coordinate system has horizontal-radial (in-line with the source azimuth), horizontal-transverse (perpendicular to the source azimuth) and vertical components. After rotation, each source offset point yields a 9-component VSP with P, SV and SH sources each recorded by vertical, horizontal-radial and horizontal- transverse receivers. An example of a 9-component data set is shown in Figure 2. The ten 9-component VSPs (one from each source site) form the survey data base.

After the data are sorted and rotated, P, SV and SH travel times are picked for first arrivals on the appropriate seismograms (the diagonal panels in Figure 2). All times are picked from the peak or trough of the zero-phase vibroseis wavelet (depending on polarity) using interactive graphics software. This travel time information forms a data base for two studies, the velocity inversion and the anisotropy measurement.

Anisotropy Measurement

The anisotropy is quantified by comparing the travel times for shear-wave arrivals from the SH- and SV-source at every depth for each site (Majer et al., 1989, Daley et al. 1989). A difference in travel time is evidence of shear-wave splitting which is caused by anisotropic S-wave propagation. Only two sites, 8 and 12, showed such difference. Figures 3 and 4 show the travel time differences for these sites, which are offset to the northeast. At both sites the SH-source generates the faster shear-wave. The depth dependence of the 40 - 50 ms differences indicates that the shear-wave splitting occurs predominantly at very shallow depths (less than 150 m). Assuming 150 m of anisotropic material with S-wave travel time of about 350 ms, we find a minimum of about 11% shear-wave anisotropy. Apparently a shallow section to the north-east is highly anisotropic. A possible cause is shallow horizontal bedding, with large variations in seismic velocity, localized to the northeast. An additional 10-15 ms time difference appears to be accumulated below 350-400 m (Figures 3 and 4) allowing for possible anisotropy of the order 5% in the deeper tuffs. Since only the NE azimuth shows this small effect, the medium at all explosive source levels is considered to be isotropic (an anisotropic medium at depth would show a continual increase in SV-SH travel-time difference with depth).

Velocity Inversion

For the velocity inversion the travel time data were projected onto 2 nearly perpendicular planes, and independent 2-D inversions were computed for each plane. Plane 1 (approximately SW-NE) includes source sites 14, 10, 6, 4, 8, and 12 (Fig 1a). Plane 2 (approximately SE-NW) includes source sites 11, 7, 4, 9 and 13 (Fig 1a). Site 4 data were included in both inversions, providing vertical velocity control at the well site.

The inversion method is based on the technique proposed by Thurber (1983) which determines the velocities at a set of discrete nodes by minimizing the travel-time residuals. Velocities between nodes are calculated by linear interpolation and raytracing is used to produce travel-times. The damped least squares methods is used in this non-linear iterative inversion to solve for velocity perturbations at each node for each iteration. The method is described in detail by Michelini and McEvilly, 1990.

For this study, an 8 x 5 (horizontal x vertical) grid of nodes was used, plus two columns of edge nodes. The initial one-dimensional starting velocity model was based on vertical travel times at site 4.

Separate inversions were performed for the P-wave velocity (Figure 5), and for the S-wave velocity (Figure 6). For the anisotropic S-wave data (sites 8 and 12), the earliest shear-wave arrival was used. The separate determinations for P- and S-wave velocities provides a measure of Vp/Vs ratio for the 2-D sections (Figure 7).

As part of the velocity inversion the raypath coverage for each cross-section is determined. The raypaths are determined separately for P- and S-waves, and they indicate the density of sampling within a given zone. Figures 8a-8d show the P- and S-wave raypaths from all the source locations for the two sections. While the region near the well is well covered by both P- and S-rays, some regions near the edges of the model have poor coverage.

The rock volume imaged by the velocity inversion contains four major geologic units (Figure 9b). The basement Paleozoic rocks are overlain by two tuff units, the Tertiary Tunnel Beds and the younger Paintbrush Tuff, and the shallow sediments are Quaternary alluvium. P-wave velocities determined by inversion are 1.0 to 1.7 km/s in the alluvium and 1.6 to 2.1 km/s in the tuffs (Figure 5). S-wave velocities are 0.5 to 1.0 km/s in the alluvium and 0.9 to 1.4 km/s in the tuffs (Figure 6). Within the Paintbrush and Tunnel Bed tuff formations we observe a west-dipping low-velocity zone (about 1.9 km/s P-wave and 1.1 km/s S-wave) in both sections east of the well at depths between 300 and 500 m.

Inferred faults, based on gravity and well control in the survey area, are shown in Figure 9a. One such fault has more than 100 m of basement offset SE of the survey well (Figure 9b). The SE-NW velocity cross-section indicates the location of this fault as high-velocity material between 0.3 km and 0.6 km depth and 0.2 km to 0 km SE offset from the well. A similar velocity increase is suggested in the SW-NE velocity section at 0 to 1 km offset to the NE.

Spectral Content

Amplitude spectra were computed for the first arrivals from the VSP data. We employed the maximum entropy spectral analysis method (Burg, 1972), since the time series containing the first arrival is short (approximately 50 samples at 2 ms sample rate) and the standard fast fourier transform can be inexact. This is a data adaptive method which leads to a spectral estimate with high resolution for short time series. Figure 10a shows the spectrum for a P-wave from site 4. The peak energy recorded near the bottom of the well is near 50 Hz, with some energy present at the high end of our source sweep (80 Hz.). The S-wave spectrum (Figure 10b) shows lower frequency content, with a peak at approximately 30 Hz and low signal level above about 50 Hz.

Reflectivity

The site characterization study was intended to identify any strong reflectors or scatterers near the well. Analysis was focused on the near-offset sources, sites 4, 6 and 8. Standard VSP processing, including aligning first arrivals and F-K filtering to remove large amplitude first arrivals, revealed two large amplitude coherent phases. A reflected S-wave arrival from below the deepest receiver (at 0.6 s time in the lowermost sensors in Figure 11) probably originates with the basement Paleozoic rocks at 691 m. The reflection is also seen in the P-wave sections. A second event is interpreted as a downgoing scattered S-to-P converted wave originating at approximately 300 m depth. Figure 11 shows the converted wave on a plot of site 4 SH-source, vertical-component data. The large relative amplitude of the S-to-P converted wave suggests a strong contrast in acoustic impedance. The well log data show variations in both sonic velocity and density at that depth, near the top of the Paintbrush tuff (Figure 12). No strong reflections within the VSP section were seen from the boundaries between alluvium and tuff and between Paintbrush and Tunnel formations. The thin Grouse Canyon Member (Figure 9) also produced no strong reflection.

Comparison of VSP and Explosion Data

The VSP sources occupied the same locations as the explosion receivers to provide data along reciprocal raypaths. While this aspect of data analysis has just begun, one example demonstrates the potential for decomposition of the recorded explosion waveform into separate arrivals using the VSP information. Figure 13 shows data for a 10 lb. explosion and for the VSP sources. The explosion receivers and VSP sources are at surface site 8, and the explosive source and VSP receivers are at about 360 m depth in the well. We see the effect of S-wave anisotropy on this path in the difference in arrival time for the direct shear-wave from the SV- and SH-sources. We can also identify both the SH and SV arrivals in the explosion waveform.

Discussion

By the end of FY 90 (the contract termination) the data acquisition and initial processing of the OSSY VSP have been completed with ten 9-component VSPs comprising the data set. The initial data analysis described here produced velocity models from travel-time inversion, defined the extent of shear-wave anisotropy and identified reflections and mode-conversions. The initial velocity model and structure are input data for the associated study of the explosion source functions. The results, representing the first phase of data analysis, show that valuable information on subsurface properties around UE-10 ITS #3 have been obtained with the VSP survey.

The next stage of data analysis will refine the velocity model to the limits of resolution (by decreasing the grid spacing in the inversion) and continue the comparison of reciprocal raypaths for explosion and VSP data. Further study of explosion and velocity data may provide detailed information on seismic wave propagation near the explosion source. Additionally, we hope to use the VSP data set to study attenuation, possibly obtaining 2-D Q models for P and S, and to study the particle motions of shear-wave arrivals for additional information on anisotropy. Finally, a remaining study is the investigation of near-surface variation in source response and an analysis of the wavefield recorded in the borehole with the data acquired at site 10 where we obtained three data sets from closely-spaced sources.

References

Burg, J.P., The relationships between maximum entropy spectra and maximum likelihood spectra, *Geophysics*, 37, 375-376, 1972.

Daley, T.M., T.V. McEvilly, and E.L. Majer, Analysis of P and S Wave Vertical Seismic Profile Data From the Salton Sea Scientific Drilling Project, *J. Geophys. Res.*, 93, B11, 13025-13036, 1988.

Daley, T.M. and T.V. McEvilly, NTS Seismic Yield Experiment: VSP Site Characterization Study (Abstract), *Seismological Research Letters,* 61, p 11, 1990.

Majer, E.L., T.V. McEvilly, F. Eastwood, and L. Myer, Fracture detection using P- and S-Wave VSPs at The Geysers geothermal field, *Geophysics,* 53, 76-84, 1988.

Michelini, A. and T.V. McEvilly, Seismological Studies at Parkfield: I. Simultaneous Inversion For Velocity Structure And Hypocenters Using Cubic B-Splines Parameterization, *Bull. of Seism. Soc. of Am.,* in press, 1990.

Thurber, C.H., Earthquake locations and three-dimensional crustal structure in the Coyote Lake area, Central California, *J. Geophys. Res.,* 88, p8226-8236, 1983.

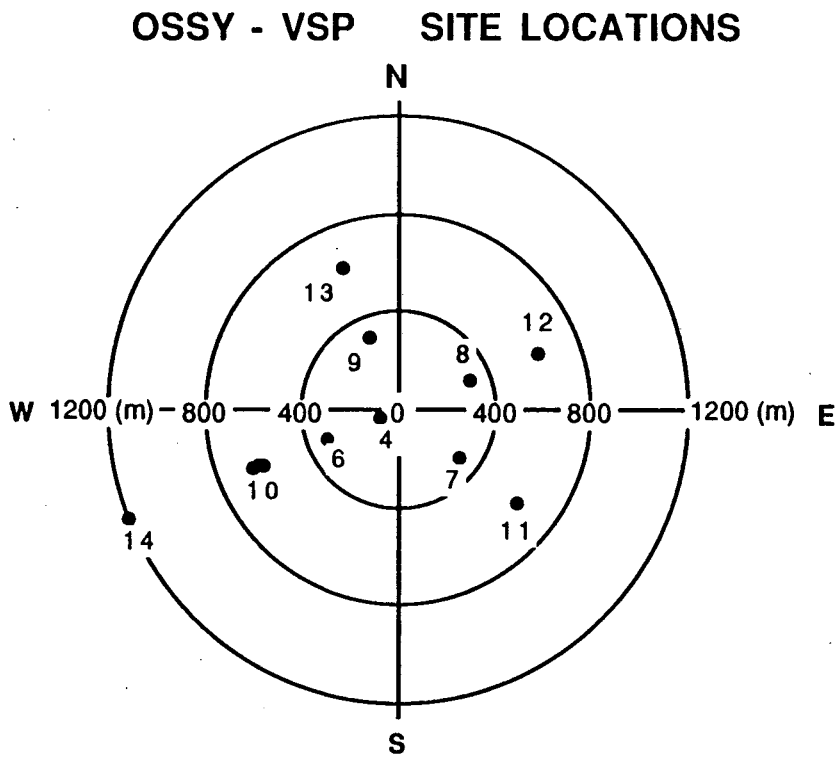

Figure 1a The source locations for each of the 10 sites. Note that site 10 has 3 closely spaced source points. The coordinate system is centered at well UE-10 ITS #3.

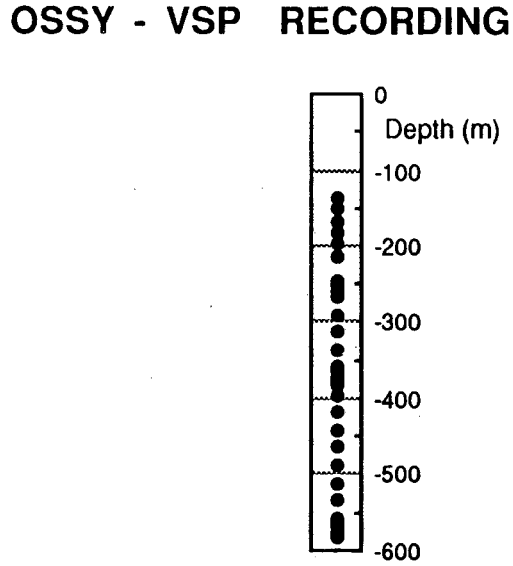

Figure 1b Receiver depths for VSP data. Note that not all receivers were recorded for every source because of acquisition time limitations and raypath consideration.

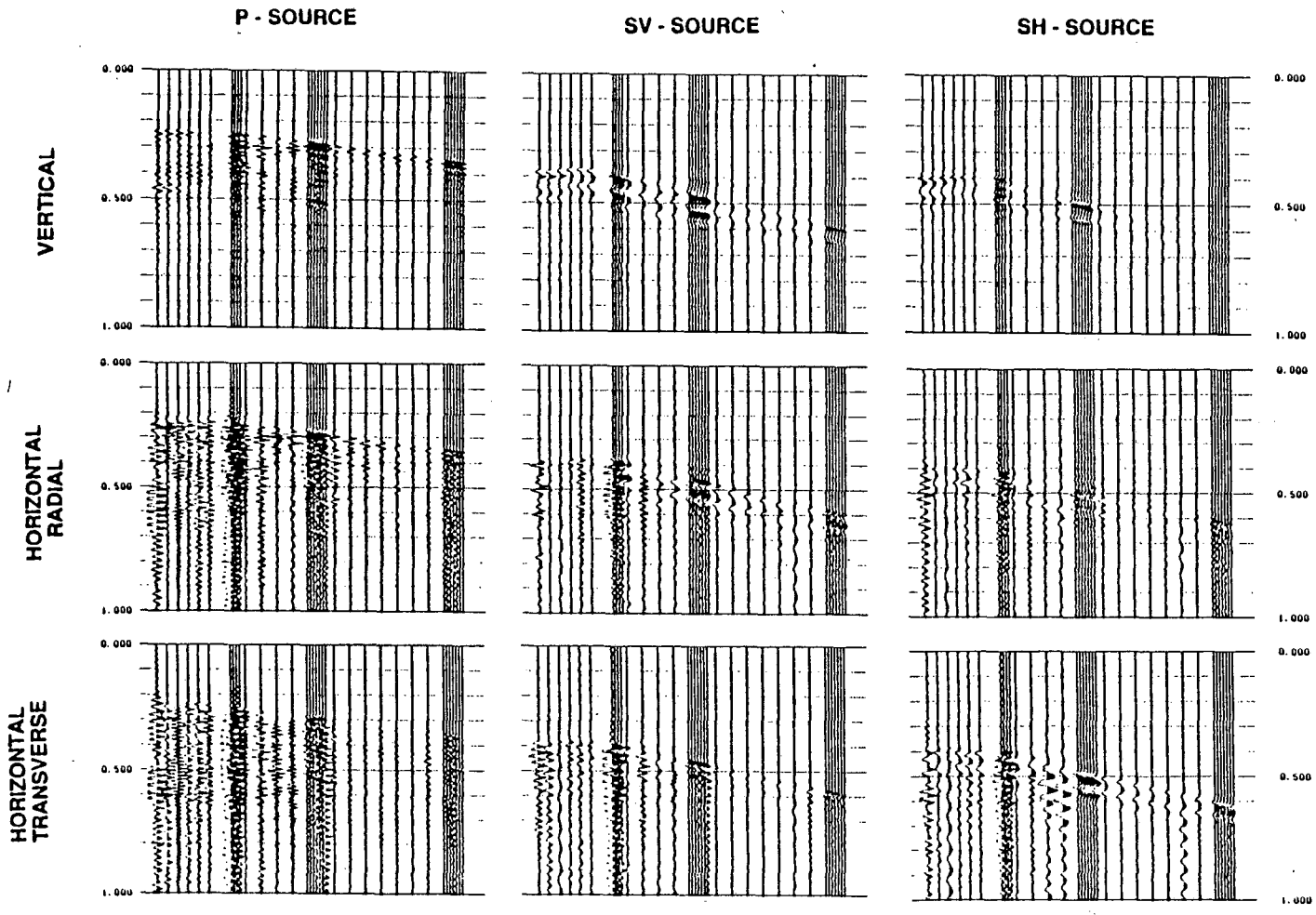

Figure 2 9-component VSP from site 6. All traces are plotted with true relative amplitude. The P-wave arrival (0.25 to 0.35 s) is best seen on the P-source vertical component, while the S-wave arrival (0.38 to 0.6 s) is clearly seen on both SV-source and SH-source data. A surface wave arrival is seen on shallow traces at about 0.48 s. The higher frequency content of the P-wave as compared to the S-wave can be seen along with the unexplained high noise level on the P-source horizontal components. The anisotropy study compares travel times of first shear-wave arrival on the horizontal-radial component of the SV-source with those on the horizontal-transverse component of the SH-source (the lower two panels in the diagonal). This data set (site 6) had no significant difference in the S-wave travel times.

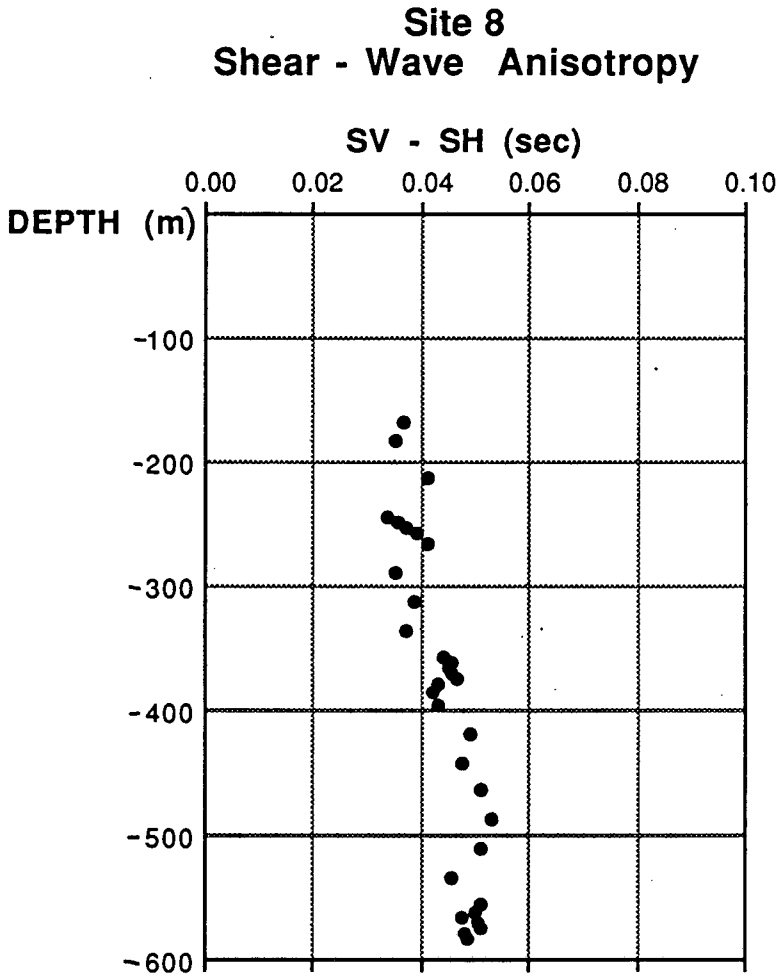

Figure 3 Plot of travel time differences between the first shear-wave for SV and SH sources (SV time minus SH time) as a function of depth for data from site 8. There is 40 to 50 ms difference at all depths; the SH-source S-wave arrival is faster.

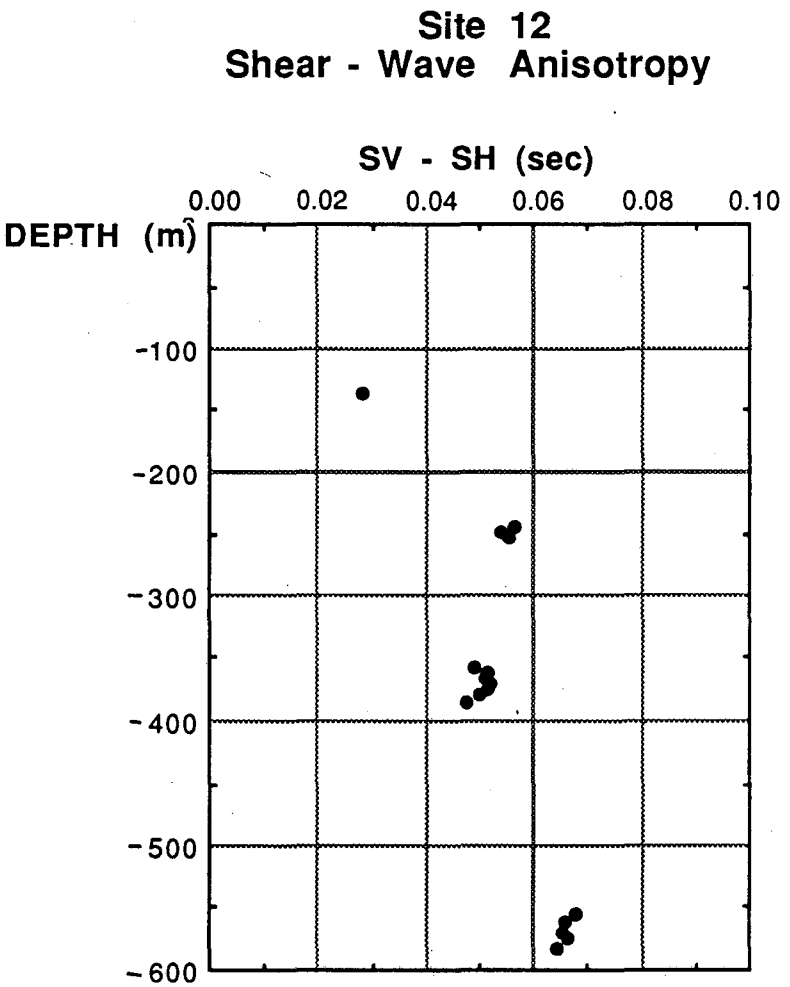

Figure 4 Plot of S-wave travel time differences for data from site 12. 30 to 60 ms difference is seen with some indication of an increase with depth. As for site 8, the SH-source S-wave arrival is faster.

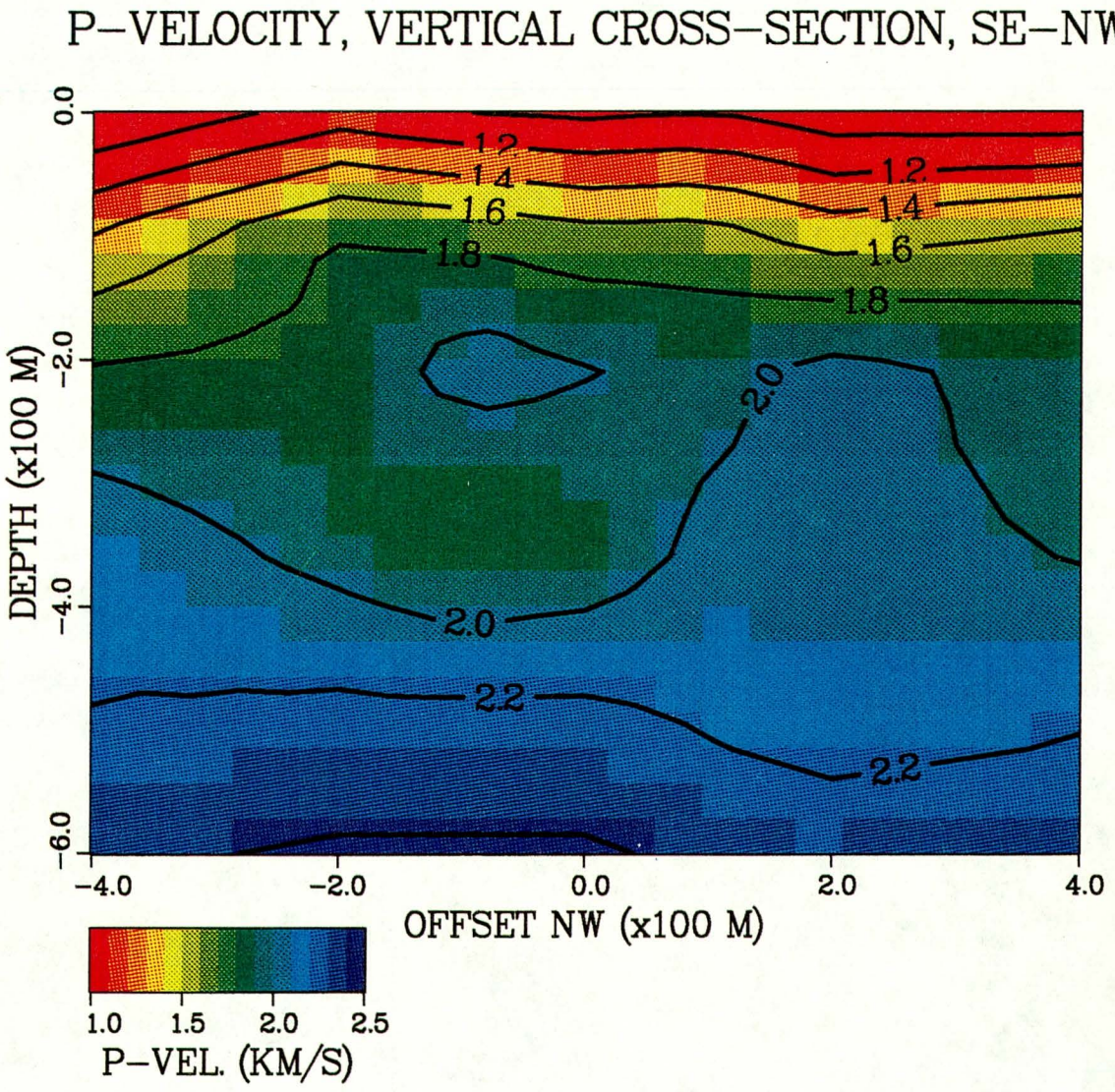

Figure 5a Results from P-wave velocity inversion in the vertical SE-NW section using data from sites 11, 7, 4, 9 and 13. The horizontal axis is centered at the well (offset =0) and extends 400 m in each direction. The steep shallow gradient defines the Quaternary alluvium. Note the higher velocities apparent at 2 to 4 km depth 100 to 300 m WN. Contour interval is 0.2 km/s.

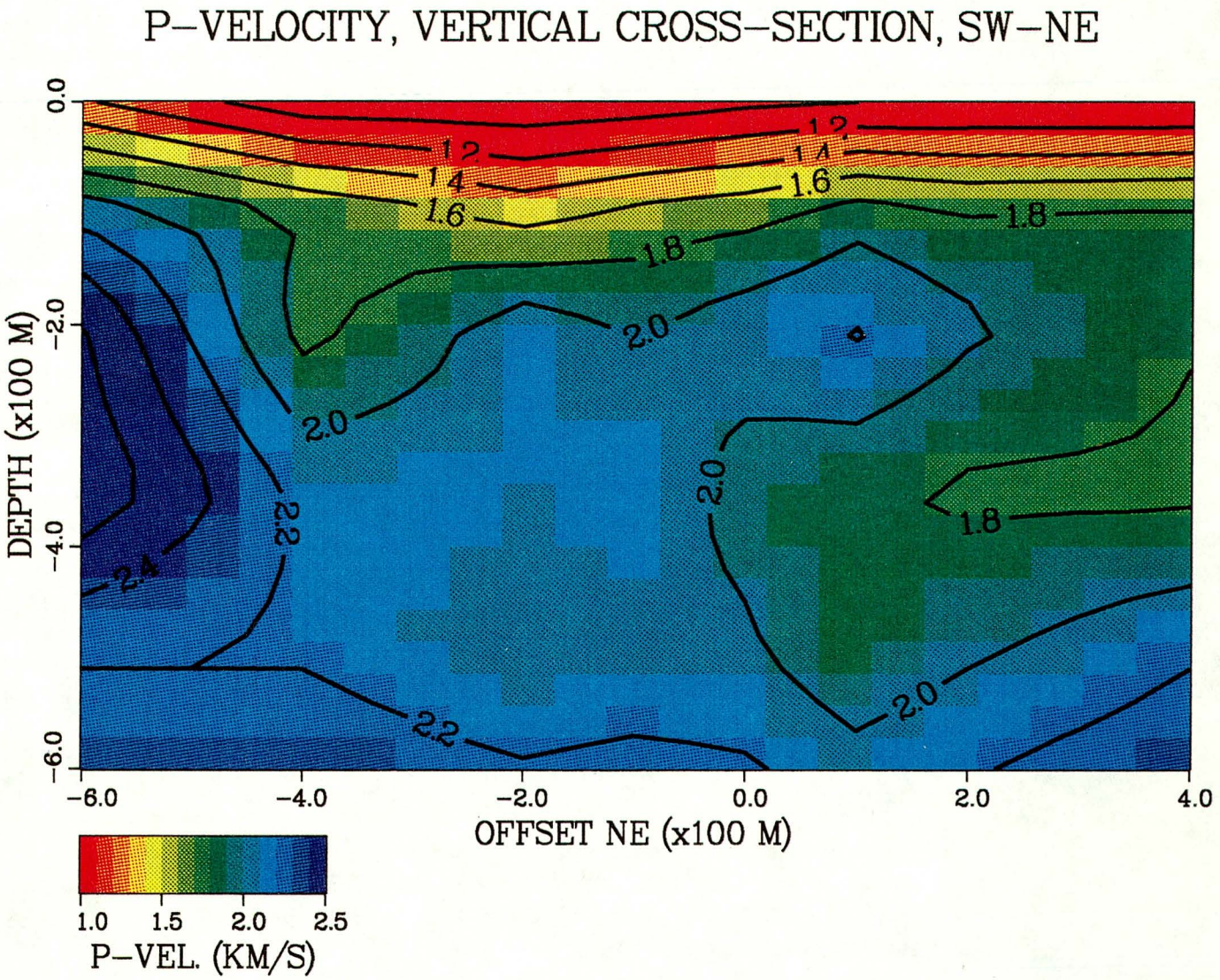

Figure 5b Results from P-wave velocity inversion in the vertical SW-NE section using data from sites 14, 10, 6, 4, 8 and 12. The horizontal axis is centered at the well (offset = 0) and extends 400 m NE and 600 m SW. The alluvium is seen as the steep gradient from 1.0 to 1.7 km/s and a SW-dipping low-velocity zone is apparent to the NE. This low-velocity zone is within the Paintbrush tuff and Tunnel beds. The high-velocity zone to the extreme SW in the model is probably an artifact of poor ray coverage. Contour interval is 0.2 km/s.

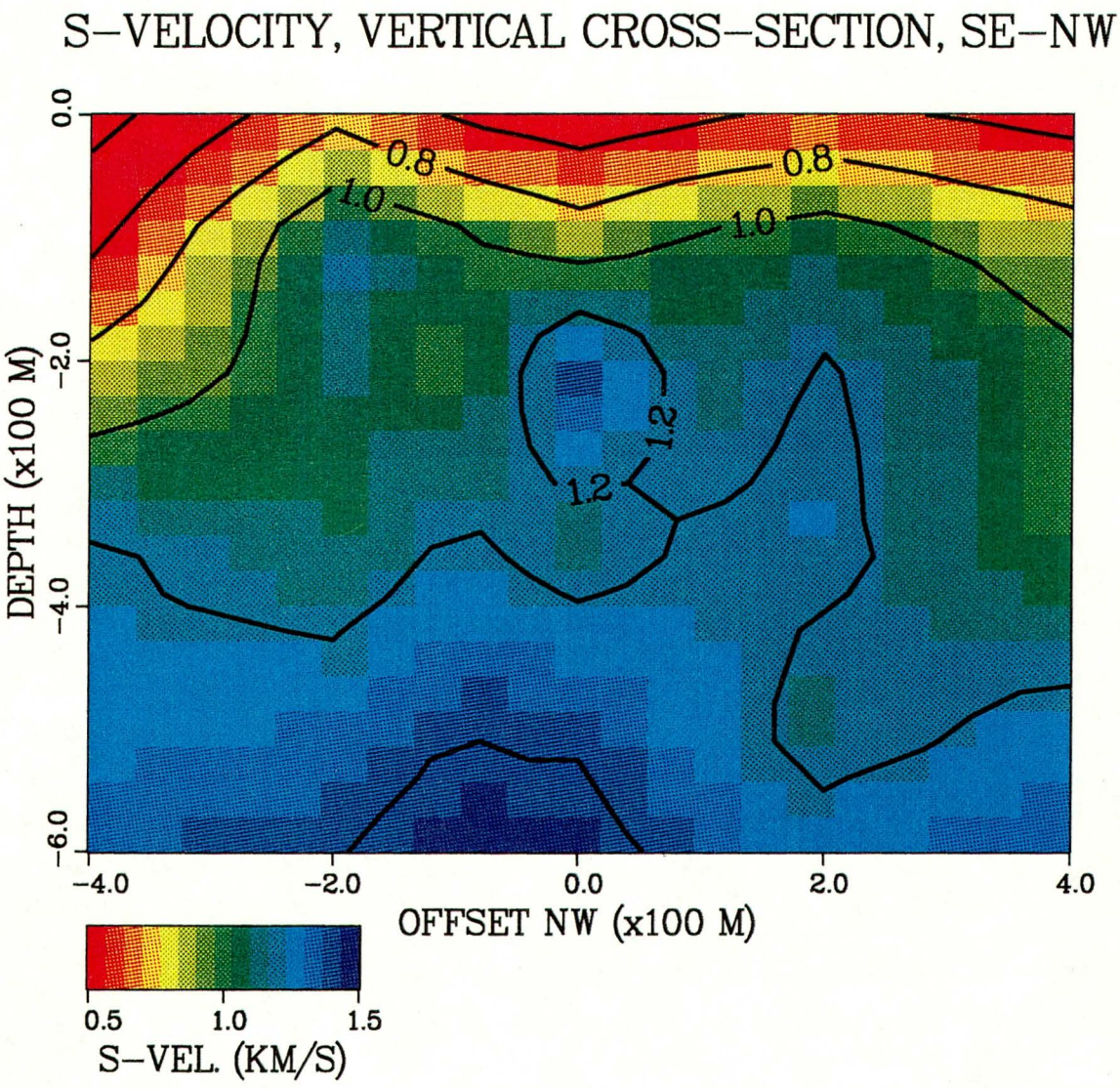

Figure 6a Results of S-wave velocity inversion in the vertical SE-NW section using data from sites 11, 7, 4, 9 and 13. The high-velocity basement feature defined by the 1.4 km/s contour is more pronounced than for the P-wave velocity model Figure 5a). Contour interval is 0.2 km/s.

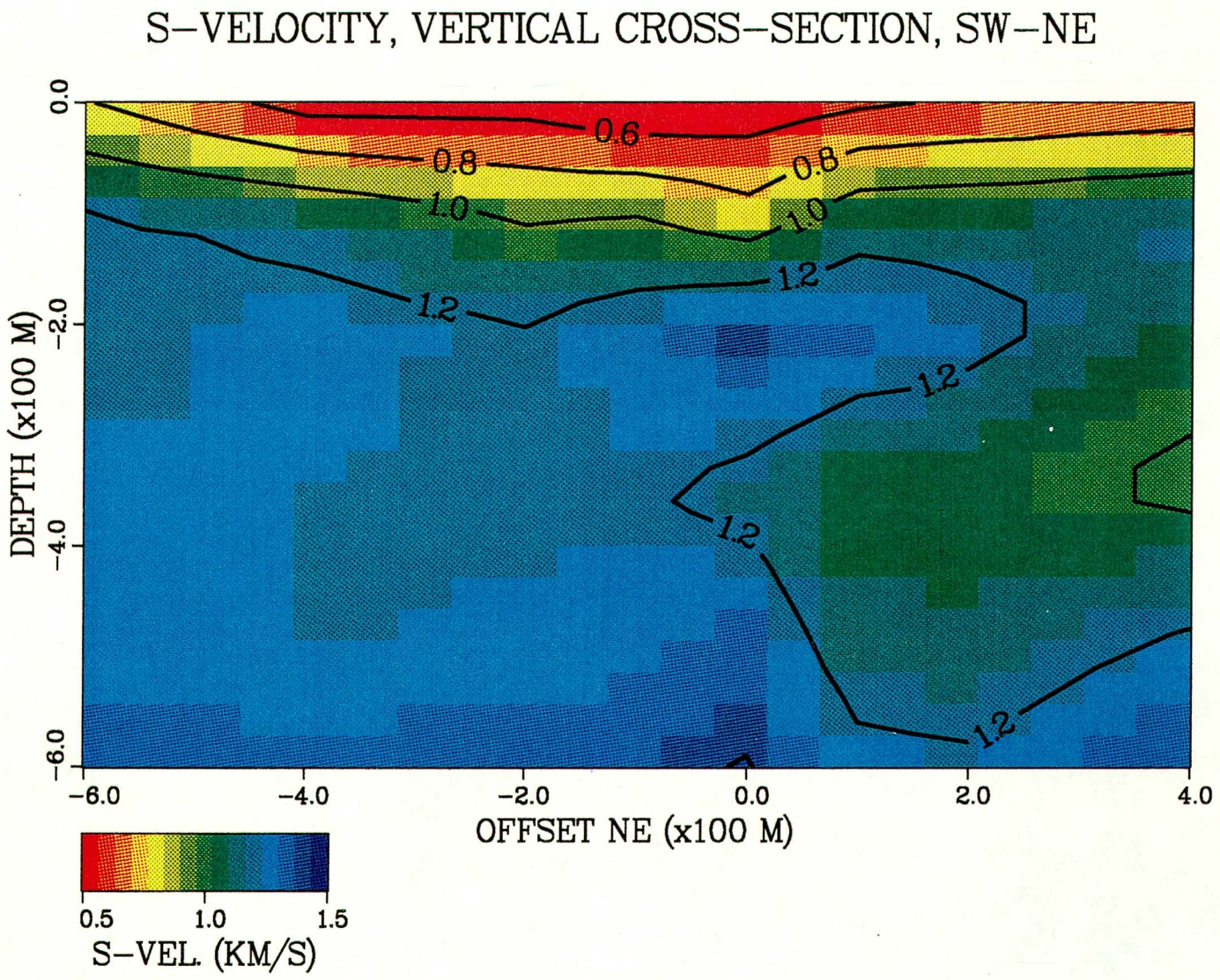

Figure 6b Results of S-wave velocity inversion in the vertical SW-NE section using data from sites 14, 10, 6, 4, 8 and 12. The dipping low velocity zone seen to the NE in the P-wave velocity inversion (Figure 5b) is also apparent here. Contour interval is 0.2 km/s.

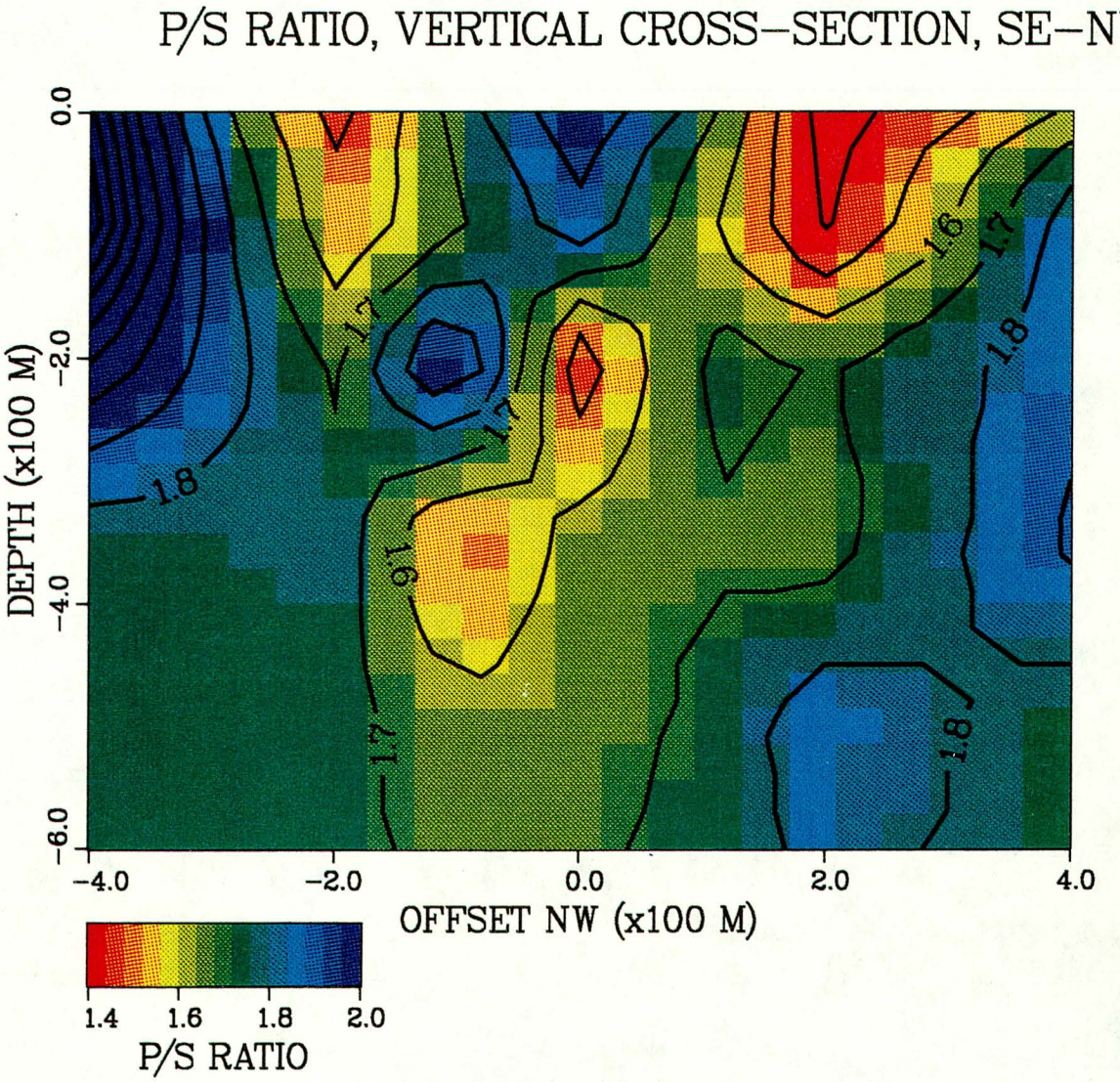

Figure 7a Vp/Vs ratio for data in Figures 5a and 6a. Most of the section has a ratio of 1.5 to 1.7, normal values for dry alluvium and tuff. Contour interval is 0.1.

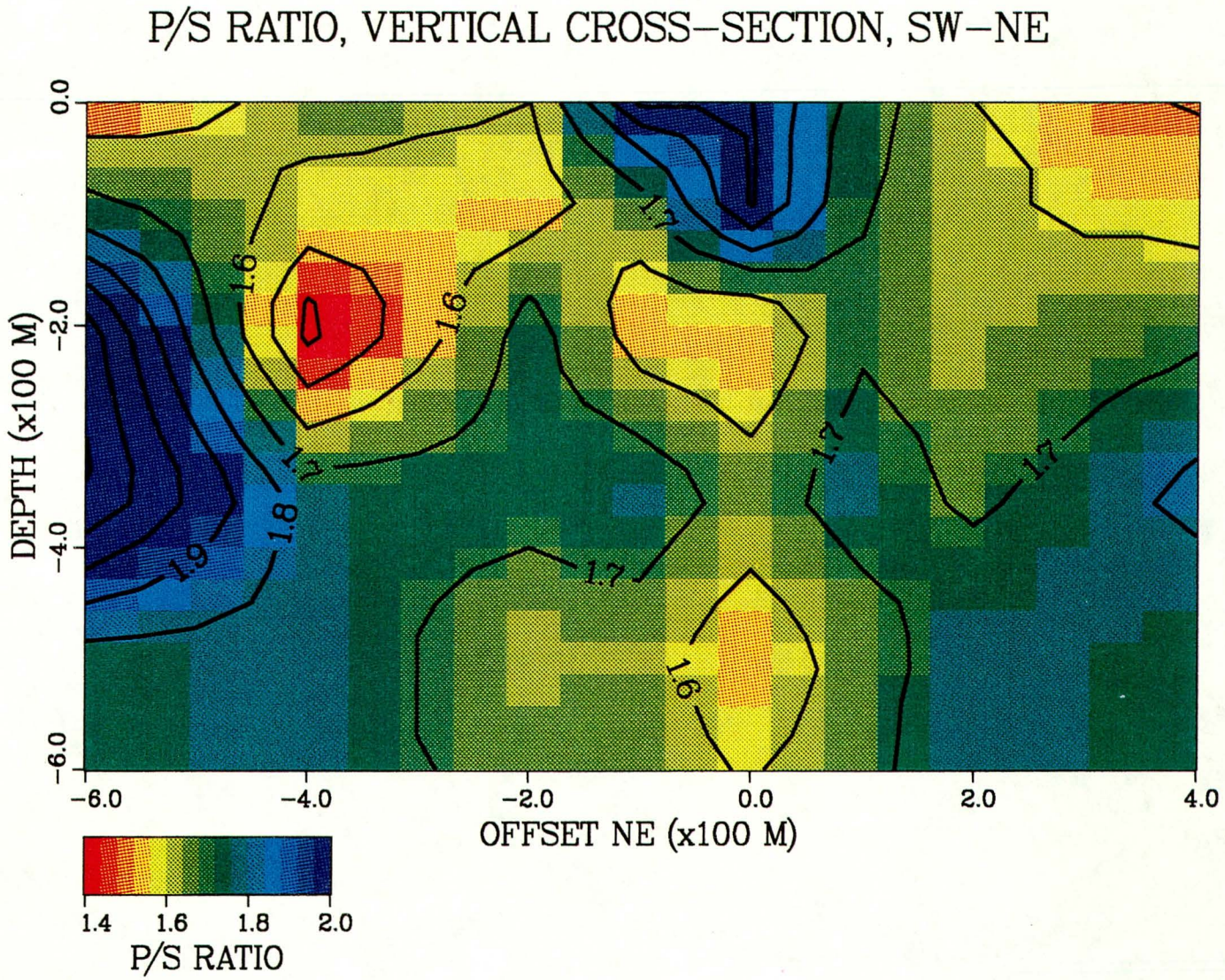

Figure 7b Vp/Vs ratio for data in Figures 5b and 6b. Contour interval is 0.1.

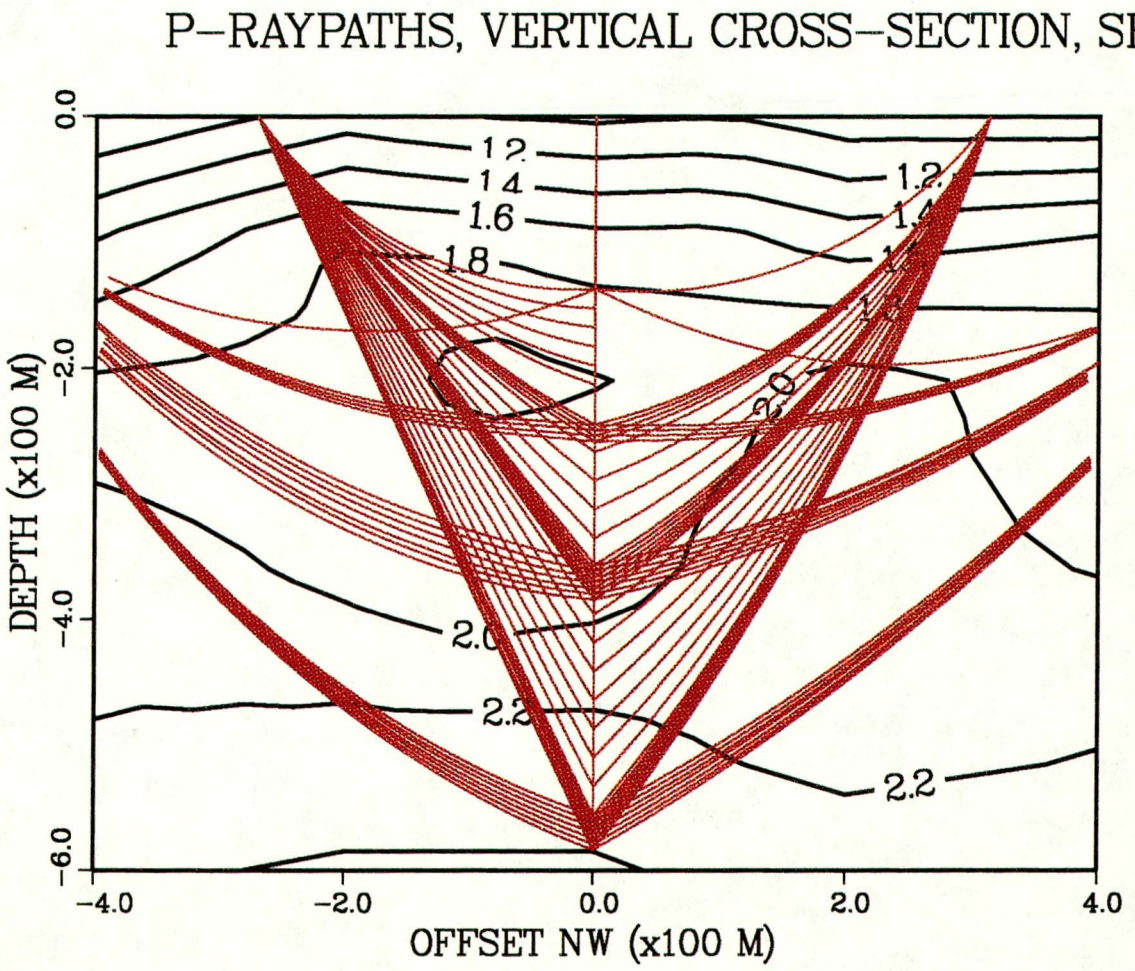

Figure 8a P-wave raypaths for sources at (left to right) sites 11, 7, 4 (vertical line at offset =0), 9 and 13. Sites 11 and 13 are outside the cross-section. Velocity contours in km/s are from P-wave inversion.

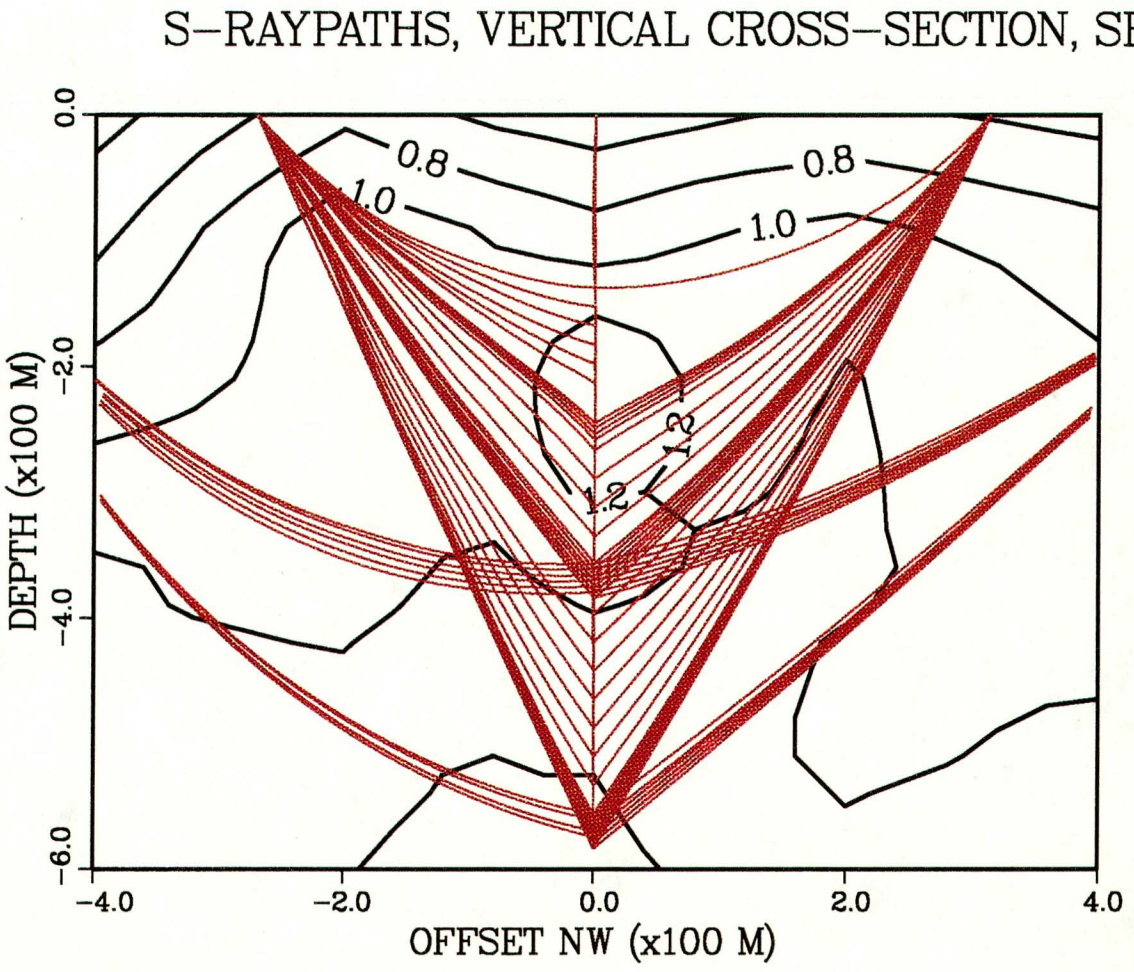

Figure 8b S-wave raypaths for sources at (left to right) sites 11, 7, 4 (vertical line at offset =0), 9 and 13 (left to right). Sites 11 and 13 are outside the cross-section. Velocity contours in km/s are from S-wave inversion in.

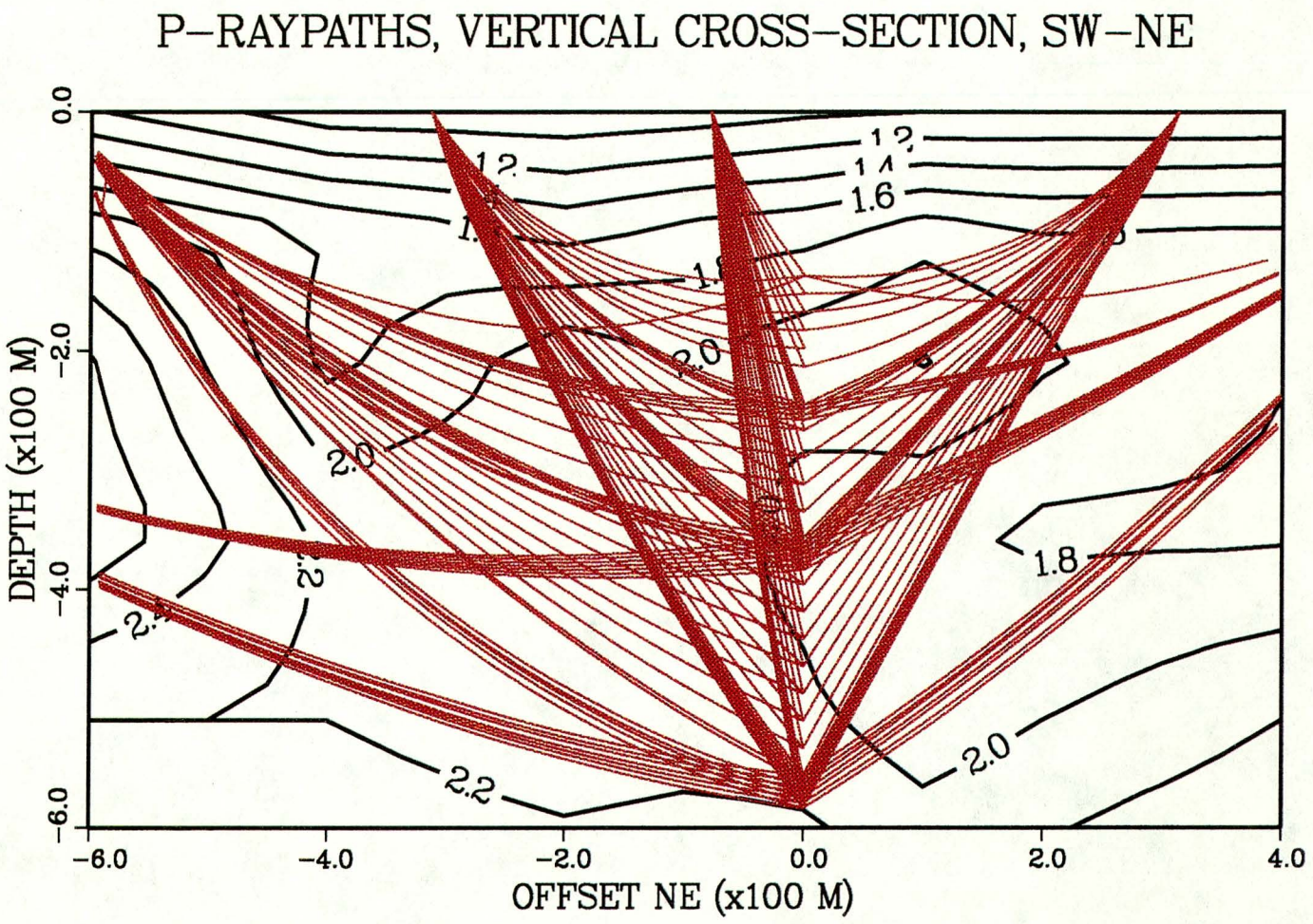

Figure 8c P-wave raypaths for sources at sites (left to right). 14, 10, 6, 4, 8, and 12. Sites 14 10 and 12 are outside the cross-section. Velocity contours in km/s are from the P-wave inversion.

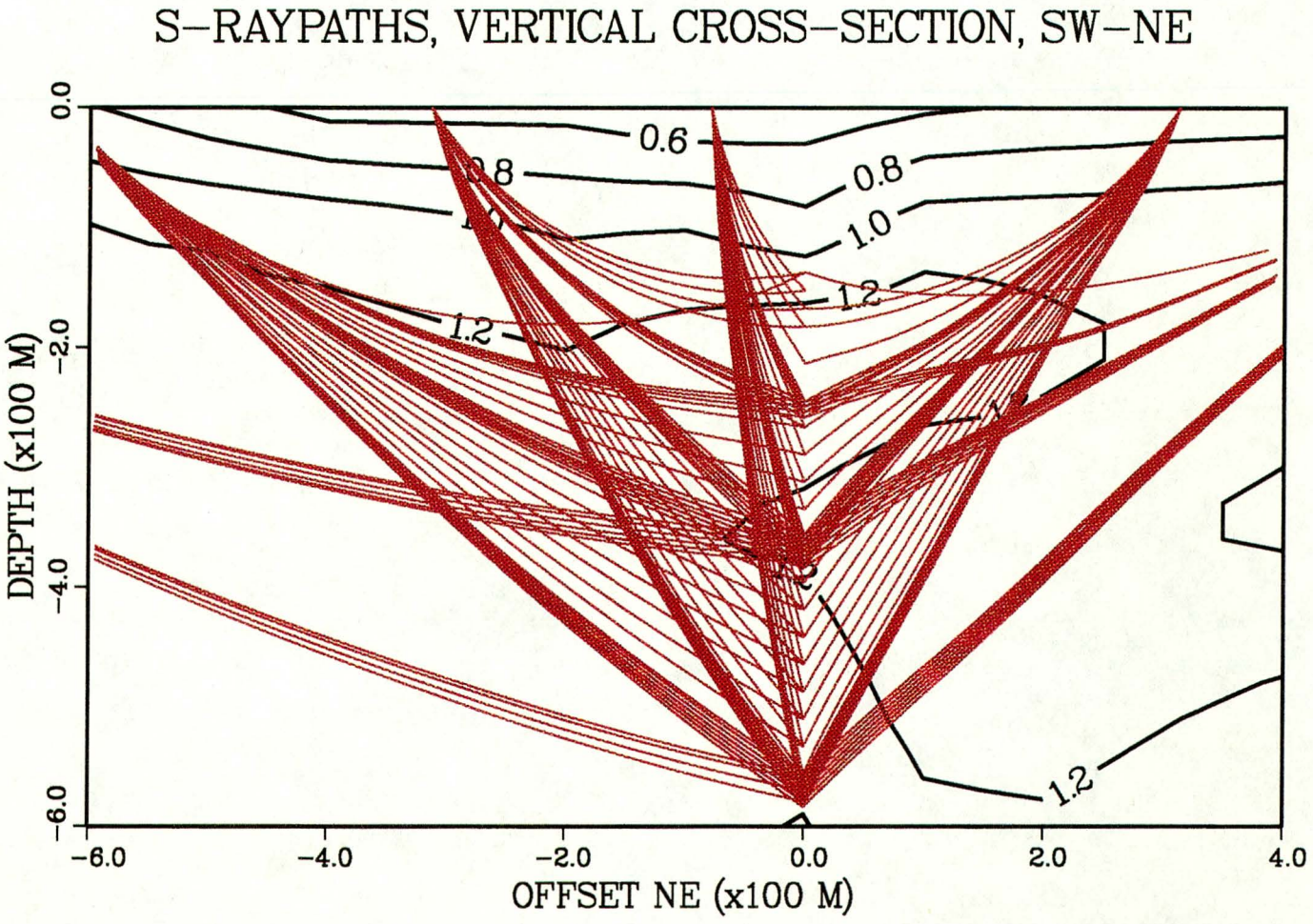

Figure 8d S-wave raypaths for sources at sites 14, 10, 6, 4, 8, and 12 (left to right). Sites 14 10 and 12 are outside the cross-section. Velocity contours in km/s are from the S-wave inversion.

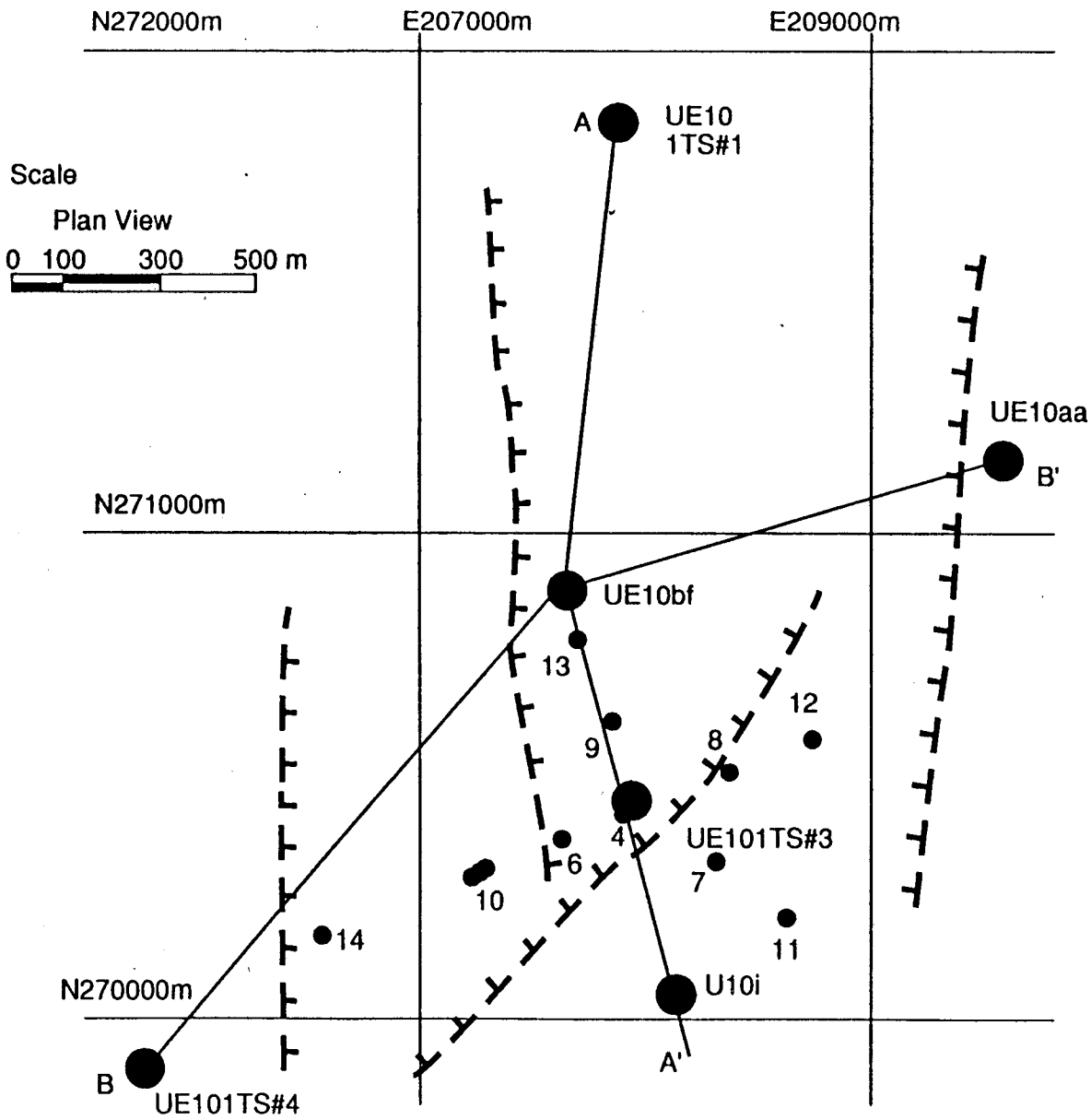

Figure 9a Survey location map with inferred faults in the study area (based on gravity data and well control) and available geologic cross-sections. Large dots are wells and small dots are VSP source locations. Geologic cross-sections A-A' and B-B' (solid lines) are shown. The OSSY-VSP used well UE10 ITS#3.

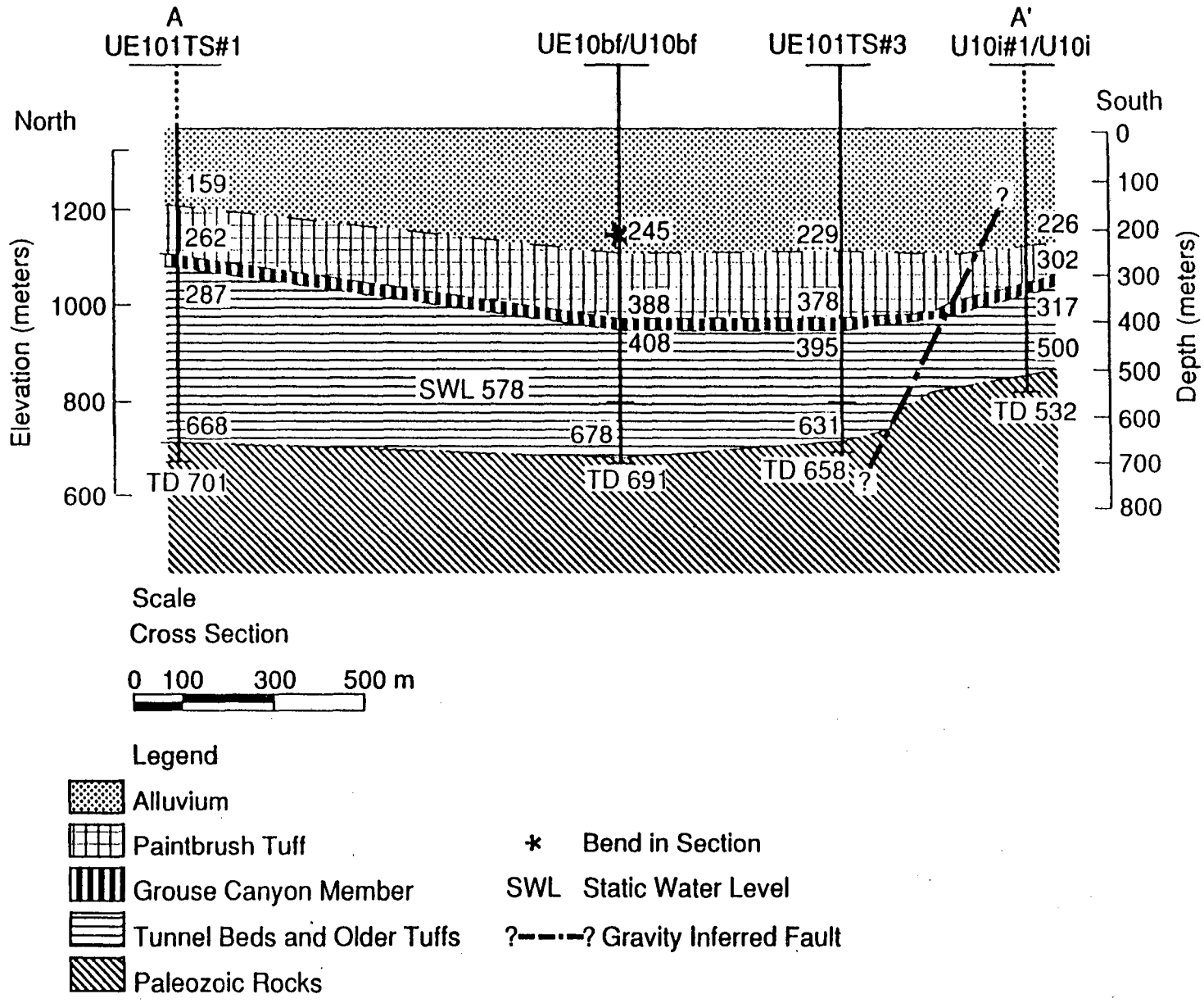

Figure 9b Geologic cross-section A-A' showing major formations in OSSY-VSP well UE10 ITS #3. The fault shown here is referred to as fault 1 in the text.

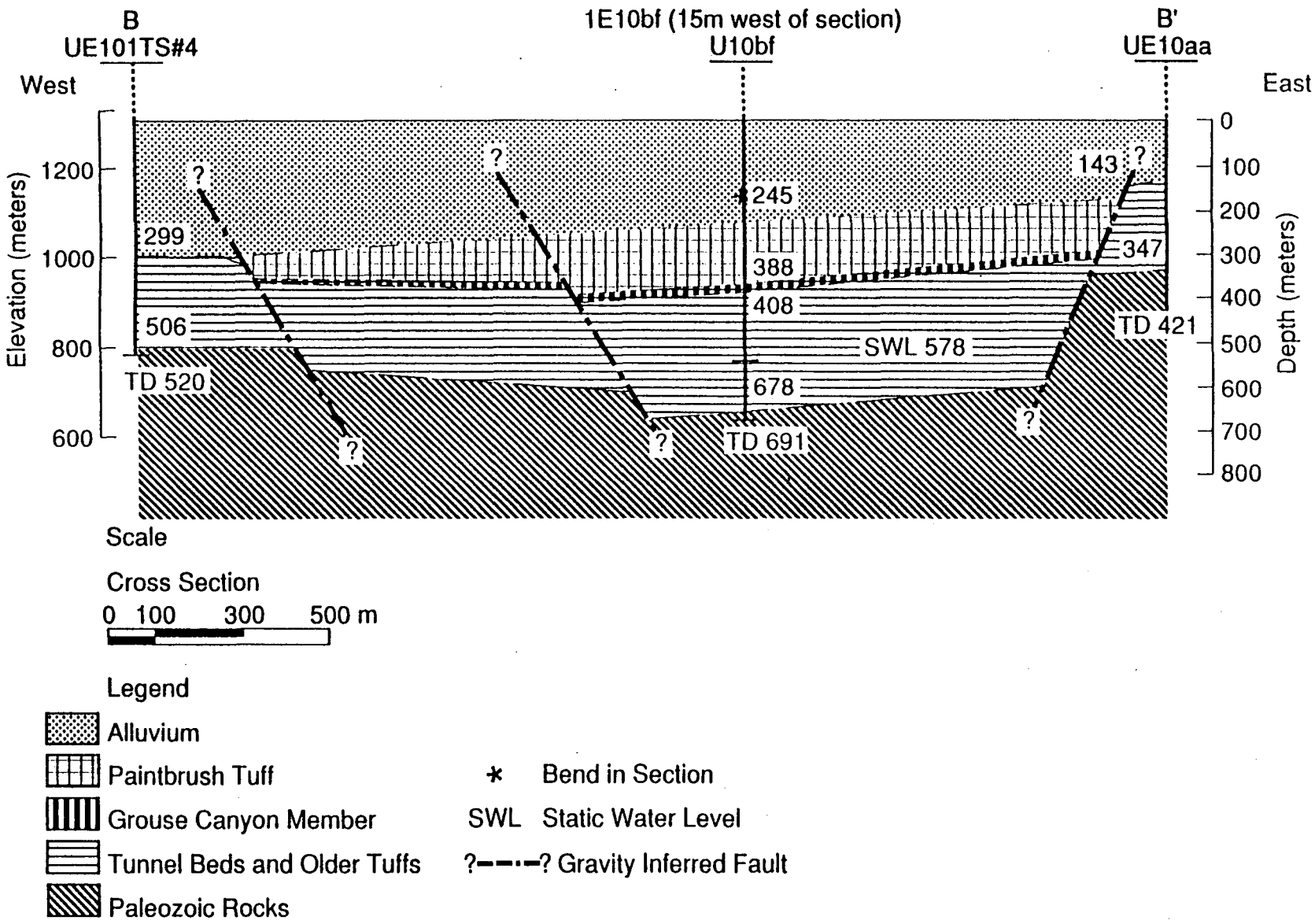

Figure 9c Geologic cross-section B-B' showing an east-west section to the north of the OSSY-VSP well (see Figure 9a).

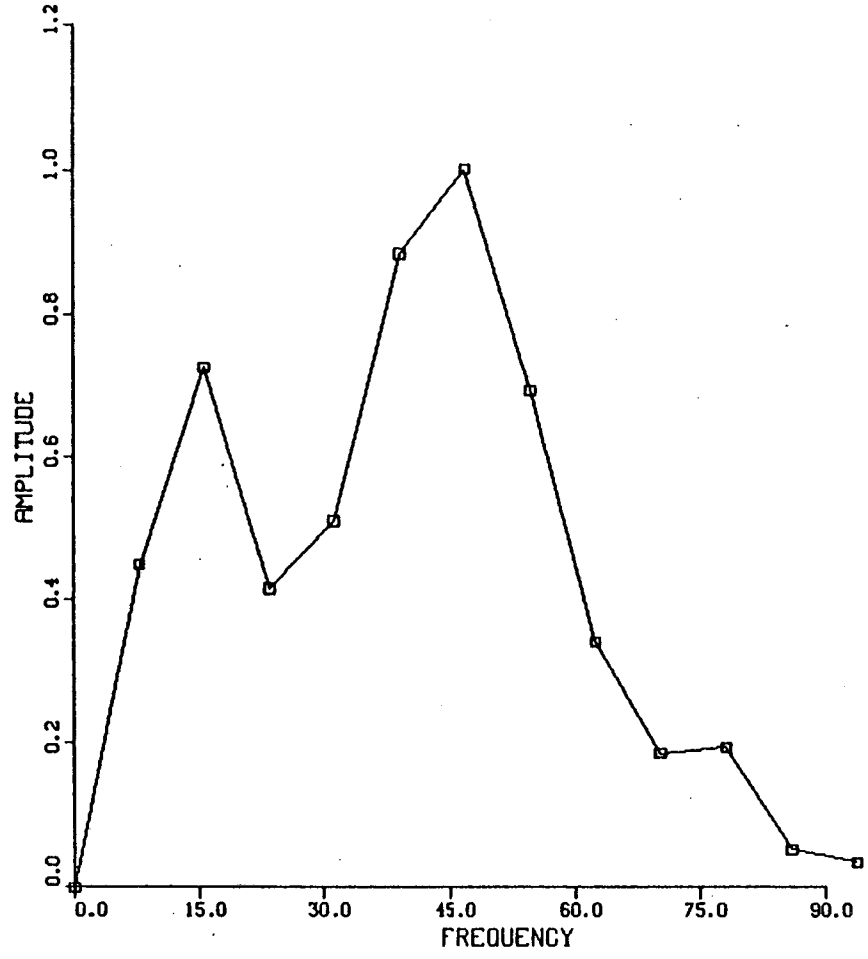

Figure 10a P-wave spectrum for the first arrival on the vertical component. The source was the P-wave vibrator at site 4 and the receiver was at 1750 m.

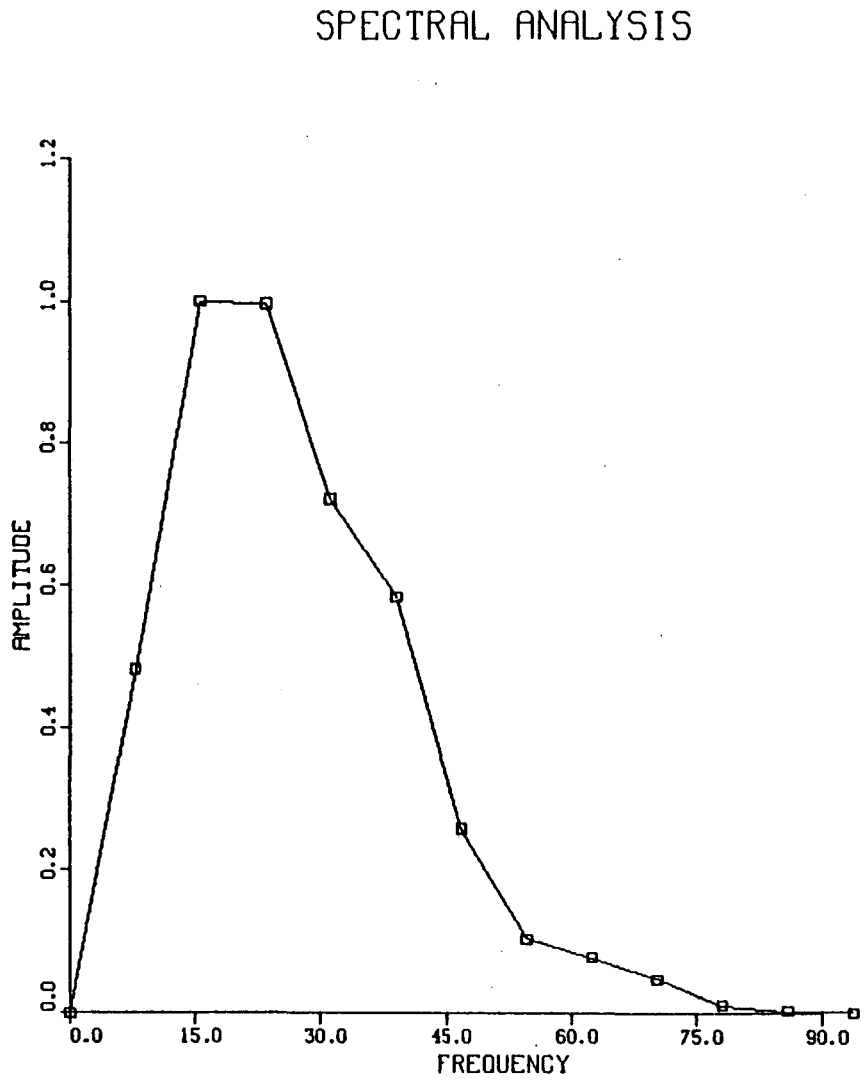

Figure 10b S-wave spectrum for the first arrival on the horizontal- transverse component. The S-wave vibrator was in the SH orientation at site 4 and the receiver was at 1915 m.

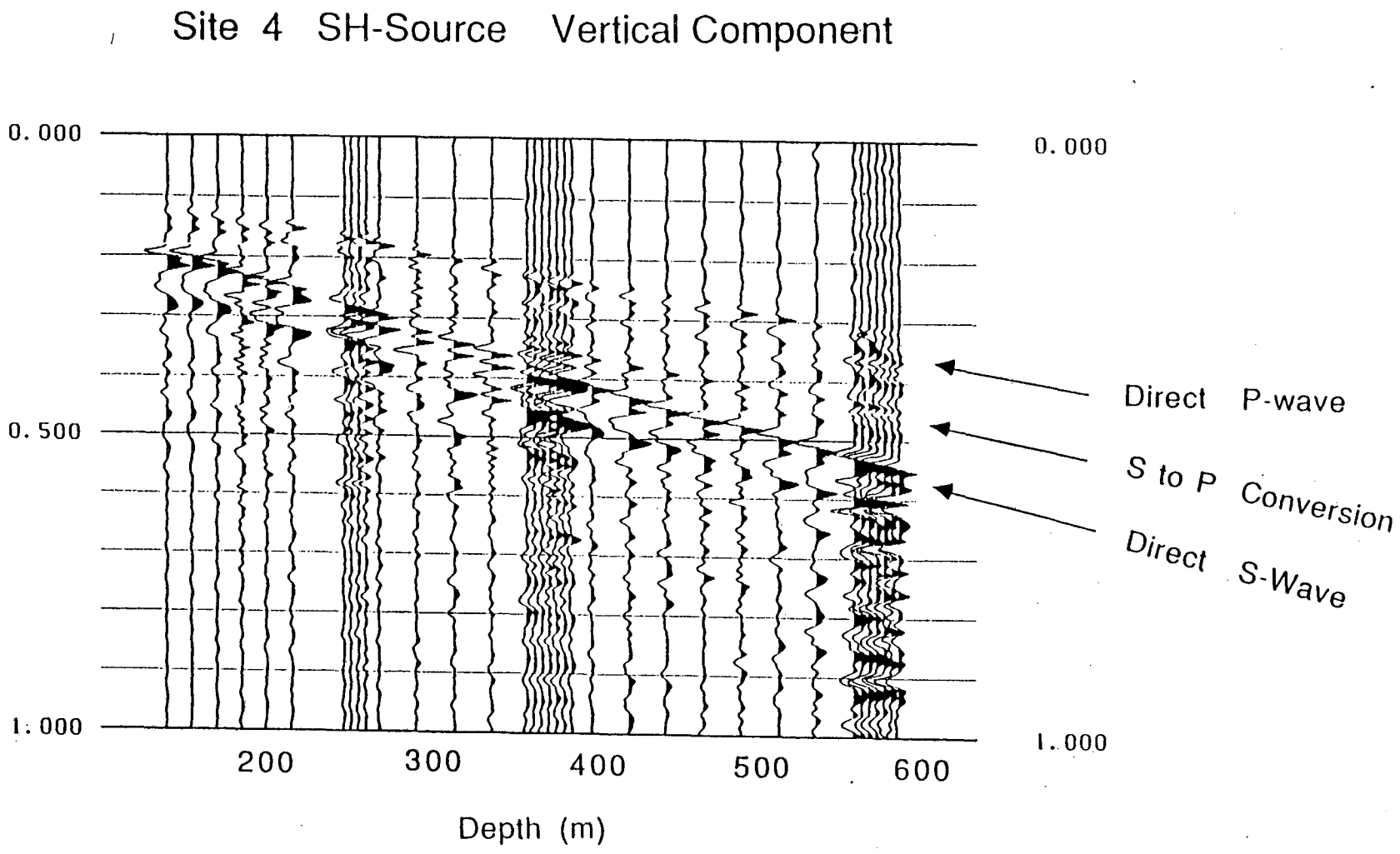

Figure 11 Data from site 4, SH-source, vertical component plotted at true depth with each trace normalized to its own maximum amplitude. The S-to-P conversion originates coincident with the direct S-wave arrival at approximately 300 m and propagates downward with the P-wave velocity. Note that the direct P-wave polarity is unstable because the SH-source is oriented tangentially to the well.

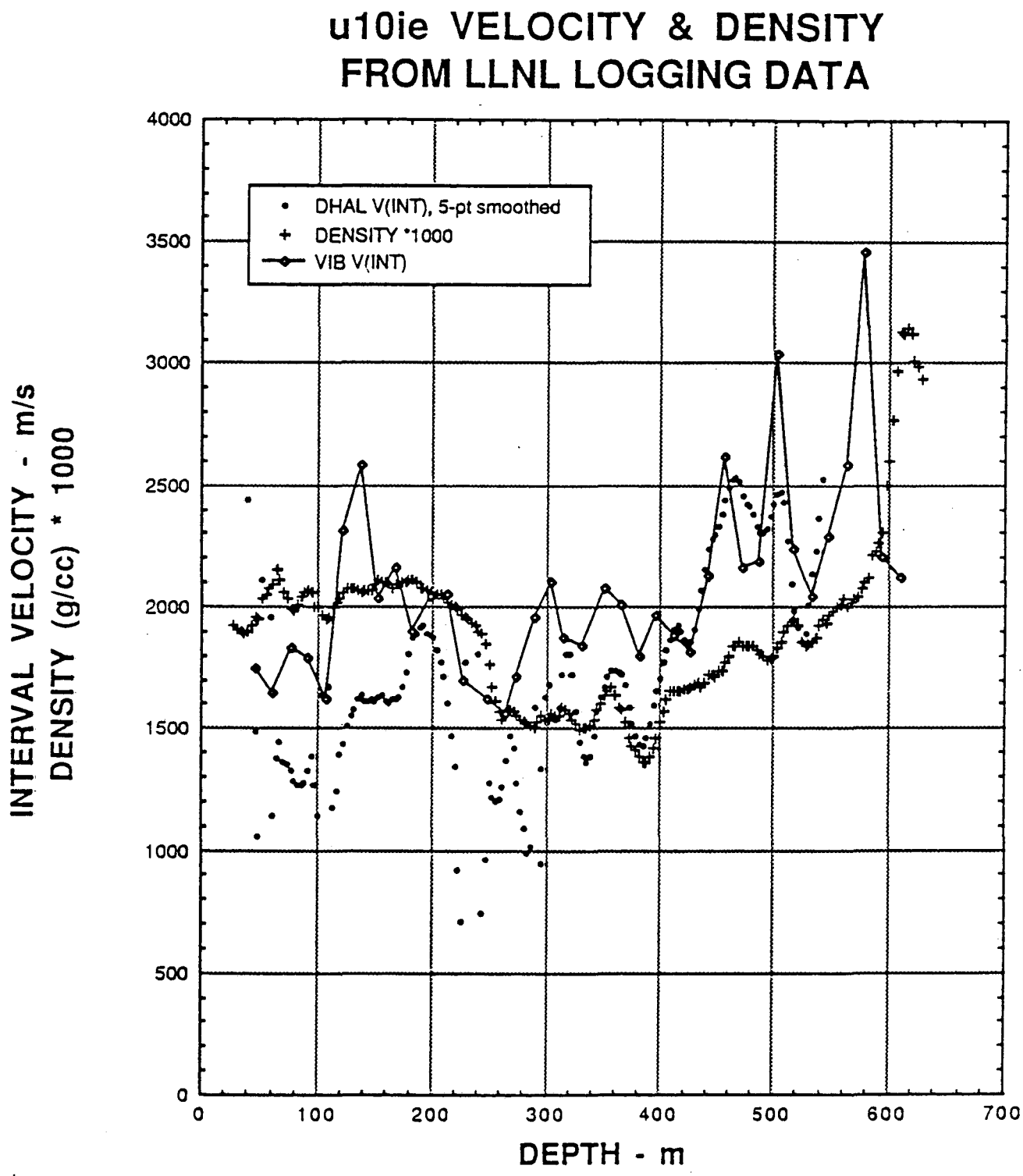

Figure 12 Well log data from UE-10 ITS #3.

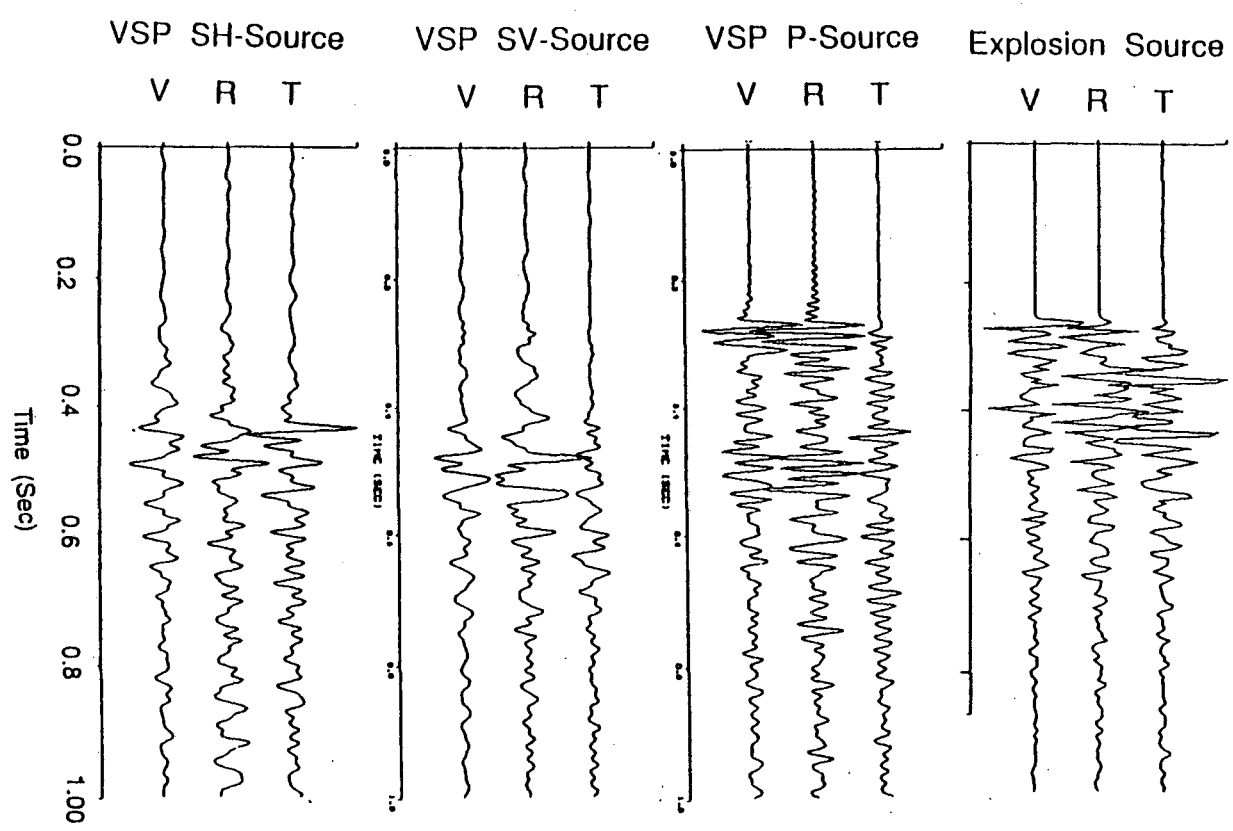

Figure 13 Comparison of 3-component data for reciprocal raypaths. The VSP data are from site 8 to a receiver at 361 m for all 3 sources. The explosion data are from a 10 lb source at 359 m to a receiver at site 8. The components are vertical (V), horizontal-radial (R), and horizontal-transverse (T). Each set of 3 components is normalized to the maximum of the 3 components. The SH-source data show a shear-wave arrival at 0.44 s with large amplitude on the transverse component and a similar arrival is seen from the explosion source. The SV-source data have a shear-wave arrival at 0.48 s demonstrating the anisotropy plotted in Figure 3. The explosion source also has an arrival at 0.48 s on the vertical and radial components. The VSP data allows accurate identification of these later arrivals in the explosion data. The explosion source data display a large arrival on the transverse component at about 0.35 s which is not seen on the VSP data; this may be a P-to-S conversion related to the S-to-P conversion seen in Figure 11.

LAWRENCE BERKELEY LABORATORY
UNIVERSITY OF CALIFORNIA
INFORMATION RESOURCES DEPARTMENT
BERKELEY, CALIFORNIA 94720